Aridity is expressed in river topography globally

Shiuan-An Chen[1]*, Katerina Michaelides[1,2], Stuart W. D. Grieve[3] and Michael Bliss Singer[2,4,5]

[1]School of Geographical Sciences, University of Bristol, Bristol, BS8 1SS, UK. [2]Earth Research Institute, University of California Santa Barbara, Santa Barbara, California 91306, USA. [3]University College London, London, WC1E 6BT, UK. [4]School of Earth and Ocean Sciences, Cardiff University, Cardiff, CF10 3AT, UK. [5]Water Research Institute, Cardiff University, Cardiff, CF10 3AX, UK.

*e-mail: sc16970@bristol.ac.uk

It has long been suggested that climate shapes land surface topography, through interactions between rainfall, runoff, and erosion in drainage basins[1-4]. The longitudinal profile of a river (elevation versus distance downstream) is a key morphological attribute that reflects the history of drainage basin evolution, so its form should be diagnostic of the regional expression of climate and its interaction with the land surface[5-9]. However, both detecting climatic signatures in longitudinal profiles and deciphering the climatic mechanisms of their development have been challenging due to the lack of relevant data across the globe, and due to the variable effects of tectonics, lithology, land-surface properties, and humans[10,11]. Here we present a global dataset of river longitudinal profiles (n = 333,502), and use it to explore differences in overall profile shape (concavity) across climate zones. We show that river profiles are systematically straighter with increasing aridity. Through simple numerical modeling, we demonstrate that these global patterns in longitudinal profile shape can be explained by hydrological controls that reflect rainfall-runoff regimes in different climate zones. The most important of these is the downstream rate-of-change in streamflow independent of drainage basin area. Our results illustrate that river topography inherits a signature of aridity, suggesting that climate is a first-order control on drainage basin evolution.

Conventional theory presents river longitudinal profiles (long profiles) as having a generally concave-up shape, with knickpoints and other fluctuations expressing the interactions of several independent variables: climate, tectonics, lithology, and human impacts[11-13]. This characteristic shape of long profiles has been interpreted to arise due to downstream flow increase with drainage area, which erodes the riverbed, transports sediment from upstream to downstream, and produces fining profiles in bed material grain size[13,14]. However, there are long profiles with overall concavity much closer to zero (straighter) than the typical concave-up profile shape[15-17], yet there is limited understanding of the global distribution of long profile concavities and their relation to climate. Stream power incision theory states that channel erosion is intrinsically tied to an assumed relationship between river discharge (Q) and drainage area ($Q \sim A^c$). Based on this theory, an expression has been derived that links supply-limited river long profile concavity to the exponent c[18], illustrating that profiles will be concave up for $c > 0$, straight for $c = 0$, and convex for $c < 0$, and a similar dependency of profile concavity on the Q-A relationship has been derived for transport-limited fluvial systems[19]. Previous work has largely emphasized long profile concavity for cases where $c > 0$, despite evidence that c in many river basins, especially in drylands, may vary flood to flood between negative, zero, and positive values[8,17,20]. Of particular interest here is to ascertain whether the climatic expression within river channel hydrology may be a first-order control on long profile shape, and whether its climatic signature is preserved across the globe.

A river experiences a cascade: from climate to hydrology to erosion, which evolves its long profile. Therefore, the climatic expression within streamflow should be a first-order control on long profile shape[6-8]. Numerical analysis of profile shape responses to a distribution of flow events above the threshold for bedrock incision has demonstrated part of this dependency[5,8,21]. However, there is limited global evidence of how the hydrologic expression of climate affects long profiles, across a wide range of climate zones. Climate determines the precipitation regime within a region. In turn, the precipitation regime controls the rate and frequency of water supply to the land surface, a proportion of which generates runoff over drainage basins, subject to losses by infiltration and evapotranspiration. Flow in rivers occurs when runoff reaches

51 the channel, with notable baseflow contributions from groundwater and subsurface drainage in humid
52 regions and potential for prolonged periods of no flow in arid channels. The flow of water within a river is
53 a key driver of landscape evolution, through the corresponding downstream force exerted on the stream bed,
54 the associated channel erosion, and the expression of local river incision at each elevation position along
55 the long profile. Therefore, we propose that the climate-streamflow relationship exerts a strong control on
56 long profiles.

57 Cimate is expressed differently in the downstream rate-of-change in streamflow between arid and humid
58 endmember rivers. In arid climates, streamflow tends to decrease downstream in all but extreme floods[22]
59 for two main reasons: 1) Low annual rainfall, limited areal coverage of rainstorms, and short duration of
60 rainfall events generates partial area runoff[23]. This results in a small proportion of basin tributaries
61 contributing streamflow to the mainstem for limited periods of time. 2) Rivers are typically ephemeral (no
62 permanent flow)[24], so channels lose water through dry, porous beds (transmission losses[22]) because water
63 tables are well below the channel[25]. Thus, the commonly assumed power law relationship between
64 streamflow and drainage area (with positive exponent c) breaks down[20] such that the long-term average
65 value of c may be negative, positive, or zero. In contrast, humid channels have perennial flow (all year
66 round), supported by baseflow from groundwater, and they accumulate flow from adjoining tributaries,
67 producing downstream increases in discharge[13] (positive c). We intuit that there is a spectrum of prevailing
68 downstream changes in streamflow across the globe based on the regional expression of climate within
69 discharge regimes (e.g., dryland hydrology, mountain front orography[5]), rather than simply on drainage
70 basin area. Given the obvious link between streamflow and riverbed erosion, we hypothesize that climatic
71 signatures are imprinted within river long profiles, superimposed upon other exogenous controls. In other
72 words, we expect a great deal of scatter typical of environmental data, but we hypothesize that climate will
73 reveal itself as a first-order control on long profile shape.

74 To test this hypothesis, we produced a new and unprecedented database of Global Longitudinal Profiles
75 (GLoPro) of rivers between 60°N and 56°S (Fig.1) extracted from NASA's 30-m Shuttle Radar

Topography Mission Digital Elevation Model (SRTM-DEM)[26]. The profiles were extracted using LSDTopoTools[27], software with advanced capabilities in topographic analysis, employing a conservative threshold for upstream drainage area and an algorithm of downstream flow accumulation, both of which reduce the likelihood of Type 1 errors (Methods). For each profile we computed the Normalized Concavity Index (*NCI*), a metric computed based solely on profile geometry (Methods; Extended Data Fig.1) that allows for standardized comparisons of river profile shapes across the globe. The *NCI* is negative if the profile is concave-up, zero if the profile is straight, and positive if the profile is convex-up.

We categorized each profile in GLoPro using the Köppen-Geiger (K-G) climate classification[28] and the quantitative Aridity Index (AI = Precipitation/Potential Evapotranspiration)[29], to investigate relationships between climate and river long profile shape and to test whether the expression of aridity is detectable in *NCI*. K-G is based on temperature and precipitation thresholds, emphasizing vegetation response to climate. AI is a scale that represents the balance between precipitation and evaporative demand, and it declines with aridity. Here we addressed the null hypothesis that there are no differences in *NCI* between climate categories. We did not censor GLoPro for any other natural or anthropogenic factors, and it includes both bedrock and alluvial rivers. We do not make any assumptions about whether the profiles are steady-state (equilibrium) or transient, but we assumed that climate categories in K-G and AI have not changed significantly over the timescales of long profile development (Methods).

The global distribution of *NCI* values does not suggest any strong geographic biases, although there are clear concentrations of convex (Southern Siberia), concave (SE Asia), and nearly straight (Arabian peninsula) rivers (Fig.1). *NCI* distributions of different climate classes (Fig.2a) overlap and display great breadth, reflecting the large sample size and the many interacting independent variables (climate, tectonics, lithology, and human factors) that affect drainage basin development. Nevertheless, statistically significant differences between distributions are evident (Extended Data Fig.5). Comparing the four main K-G climate zones, all *NCI* distributions are negatively skewed, revealing that river long profiles are generally concave-up (Fig.2a). However, compared to the other three main climate zones (Tropical, Temperate, and

Cold), the *NCI* values for Arid zone rivers are notably closer to zero (straighter) with a narrower distribution (Extended Data Table 1). The distinct signature of straighter profiles within the Arid K-G zone in GLoPro is an unprecedented finding. To further explore this result, we investigated the relationship between *NCI* for the AI climate classification, ranging from Humid to Hyper-arid categories. We found a systematic increase in *NCI* distribution medians from concave-up to straighter profiles as aridity increases (Fig.2c,d). Furthermore, we found (Fig.2e) a higher frequency of concave river profiles within humid regions (combined Dry sub-humid and Humid AI categories), and a higher frequency of straighter profiles in drylands (combined Hyper-arid, Arid, and Semi-arid AI categories). In other words, the straightness of the long profile appears to be directly related to the water balance of a region, and by extension its expression within streamflow regimes that erode riverbeds.

Why are arid river long profiles straighter than humid ones, and how does climate influence the long profile through its expression in streamflow? Stream power theory indicates that the variation of discharge with drainage area influences long profile concavity for supply-limited channels. We sought to relax this assumption of Q-A dependency and thus provide a more general mechanistic explanation of our GLoPro results, and one which applies to transport-limited channels. We used the numerical model, LONGPRO[30] (Methods), and distilled the hydrological expression of climate within a parameter representing the downstream rate-of-change in streamflow, which replaces the Q-A relationship from stream power theory. Specifically, discharge changes with distance down the channel at a rate controlled by the power law exponent, α, in the equation: $Q_L = Q_n (L/L_n)^{\alpha}$, where Q_L is the discharge at a distance downstream, L, and n is the most downstream point on the profile (Methods). We simulated the evolution of river long profiles with six values of α representing a range of downstream decreasing and increasing discharge rates ($\alpha = -2, -1, -0.5, 0.5, 1, 2$). We kept all other LONGPRO model parameters constant within established ranges for natural rivers but we separately explored their influence on *NCI* (Methods). For each simulated profile, we calculated the *NCI* value (Fig.3a).

We found that *NCI* in the simulated profiles is systematically influenced by α (Fig.3b). Specifically, the fastest downstream decreasing discharge ($\alpha = -2$) produces convex-up profiles and profiles become progressively straighter and then concave-up with increasing α. In general, long profiles are straighter when α approaches zero (discharge does not vary downstream). These LONGPRO results provide definitive mechanistic support to our *NCI* results from GLoPro, and they also corroborate the effect of the exponent *c* on concavity from stream power theory, pointing to aridity and its influence on downstream discharge as a first-order control on longitudinal profile shape.

We tested the representativeness of the modeled α values for real rivers by analyzing flow data from a range of gauged US rivers (Methods). The analysis reveals ranges of α consistent with expectations for each K-G climate zone, whereby Tropical, Temperate and Cold zones exhibit large, positive α values, and the Arid zone displays α values close to zero (Extended Data Fig.8a). Note that a range of α values (positive, negative, and zero) are probably common to arid rivers due to the variable expression of climate within stream hydrology on a flood-by-flood basis[17,20]. Furthermore, the mean value of α is affected by long periods of no flow (ephermerality), typical of dryland rivers (Extended Data Fig.8b). Ephemerality accentuates transmission losses that reduce downstream flow and also gives more weight to each historical flood event, wherein smaller floods that exhibit downstream decreasing discharge are more frequent, yet less geomorphically effective than large ones that increase downstream[4,17]. Thus, α may vary between negative and positive values for each flood, resulting in a distributional mean value close to zero.

Combining these hydrologic data with our model results enables interpretation of the global trends in long profile concavities with aridity. The results demonstrate three things: 1) The concave-up river profile can develop based solely on perennial flow conditions and downstream flow increase, consistent with stream power incision theory[18]. 2) Straighter long profiles can evolve in rivers that flow infrequently, and where over the long term, the median discharge is similar everywhere along the channel. 3) Convex long profiles can develop under a range of ephemeral/perennial conditions, but where climate may not be the first-order control. All of these profile shapes exist within GLoPro (Figs.1;2) with a preponderance of

concave-up profiles in all climate zones (modeled large positive α), numerous straight profiles concentrated in arid regions (modeled small $|\alpha|$), and a smaller set of convex-up river profiles (modeled negative α) occurring in humid (strong orographic effects[5]) and arid regions (partial area contribution[23] and transmission losses[22]). The effect of α in transport-limited rivers (and by extension, c in supply-limited rivers) overprints other plausible controls on profile concavity on the global scale (Extended Data Fig.6).

Our new global dataset, GLoPro, combined with simple numerical modeling and hydrological data analysis has provided a new explanation of how the hydrological expression of climate can produce systematic differences in long profile shapes based on aridity. From this first global analysis of longitudinal profiles, we demonstrate that climatic signals are etched into river long profiles irrespective of the variety of environmental conditions and other forcings across the globe (Methods). Despite overlaps in the *NCI* distributions, the overriding signal is one of aridity affecting channel flow and the cascade from climate to hydrology to erosion, corroborating previous studies[8,10,31-33]. The findings highlight the importance of hydrological regimes, directly affected by climate, as a first-order control on the development of river topography, which can enhance our understanding of drainage basin evolution in response to climate and climate change.

1. Tucker, G. E. & Slingerland, R. Drainage basin responses to climate change. *Water Resour. Res.* **33**, 2031-2047 (1997).
2. Ferrier, K. L., Huppert, K. L. & Perron, J. T. Climatic control of bedrock river incision. *Nature* **496**, 206-209 (2013).
3. Perron, J. T., Richardson, P. W., Ferrier, K. L. & Lapôtre, M. The root of branching river networks. *Nature* **492**, 100-103 (2012).
4. Wolman, M. G. & Gerson, R. Relative scales of time and effectiveness of climate in watershed geomorphology. *Earth Surf. Process.* **3**, 189-208 (1978).
5. Roe, G. H., Montgomery, D. R. & Hallet, B. Effects of orographic precipitation variations on the concavity of steady-state river profiles. *Geology* **30**, 143-146 (2002).

6. Han, J., Gasparini, N. M., Johnson, J. P. & Murphy, B. P. Modeling the influence of rainfall gradients on discharge, bedrock erodibility, and river profile evolution, with application to the Big Island, Hawai'i. *J. Geophy. Res. Earth Surf.* **119**, 1418-1440 (2014).
7. Zaprowski, B. J., Pazzaglia, F. J. & Evenson, E. B. Climatic influences on profile concavity and river incision. *J. Geophy. Res. Earth Surf.* **110**, https://doi.org/10.1029/2004JF000138 (2005).
8. Sólyom, P. B. & Tucker, G. E. Effect of limited storm duration on landscape evolution, drainage basin geometry, and hydrograph shapes. *J. Geophy. Res. Earth Surf.* **109**, https://doi.org/10.1029/2003JF000032 (2004).
9. Collins, D. & Bras, R. Climatic and ecological controls of equilibrium drainage density, relief, and channel concavity in dry lands. *Water Resour. Res.* **46**, https://doi.org/10.1029/2009WR008615 (2010).
10. Harel, M-A., Mudd, S. & Attal, M. Global analysis of the stream power law parameters based on worldwide ^{10}Be denudation rates. *Geomorphology* **268**, 184-196 (2016).
11. Hack, J. T. *Studies of longitudinal stream profiles in Virginia and Maryland*. **294B** (US Government Printing Office, Washington, 1957).
12. Phillips, J. D. & Lutz, J. D. Profile convexities in bedrock and alluvial streams. *Geomorphology* **102**, 554-566 (2008).
13. Leopold, L. B. & Wolman, M. G. *Fluvial Processes in Geomorphology*. (General Publishing, Toronto, 1964).
14. Snow, R. S. & Slingerland, R. L. Mathematical modeling of graded river profiles. *J. Geology* **95**, 15-33 (1987).
15. Vogel, J. Evidence of past climatic change in the Namib Desert. *Palaeogeogr. Palaeoclimatol. Palaeoecol.* **70**, 355-366 (1989).
16. Singer, M. B. & Michaelides, K. How is topographic simplicity maintained in ephemeral dryland channels? *Geology* **42**, 1091-1094 (2014).
17. Michaelides, K., Hollings, R., Singer, M. B., Nichols, M. H. & Nearing, M. A. Spatial and temporal analysis of hillslope–channel coupling and implications for the longitudinal profile in a dryland basin. *Earth Surf. Process. Landf.* **43**, 1608-1621 (2018).
18. Whipple, K. X. & Tucker, G. E. Dynamics of the stream-power river incision model: Implications for height limits of mountain ranges, landscape response timescales, and research needs. *J. Geophys. Res. Solid Earth* **104**, 17661-17674 (1999).
19. Tucker, G. E. & Bras, R. L. Hillslope processes, drainage density, and landscape morphology. *Water Resour. Res*. **34**, 2751-2764 (1998).

20. Wickert, A. D. How should we estimate river discharge from drainage area?, Abstract (EP21D-2294) presented at 2018 AGU Fall Meeting, Washington, D.C., 10-14 Dec (2018).
21. Lague, D., Hovius, N. & Davy, P. Discharge, discharge variability, and the bedrock channel profile. *J. Geophy. Res. Earth Surf.* **110**, https://doi.org/10.1029/2004JF000259 (2005).
22. Knighton, A. & Nanson, G. Distinctiveness, diversity and uniqueness in arid zone river systems. *Arid Zone Geomorphology: Process, Form and Change in Drylands (2nd Edition).* 185-203 (John Wiley & Sons, 1997).
23. Yair, A., Sharon, D. & Lavee, H. An instrumented watershed for the study of partial area contribution of runoff in the arid zone. *Z. Geomorphol. Suppl.* **29**, 71-82 (1978).
24. Jaeger, K. L., Sutfin, N. A., Tooth, S., Michaelides, K. & Singer, M. Geomorphology and sediment regimes of intermittent rivers and ephemeral streams. *Intermittent Rivers and Ephemeral Streams*. 21-49 (Elsevier, 2017).
25. Fan, Y., Li, H. & Miguez-Macho, G. Global patterns of groundwater table depth. *Science* **339**, 940-943 (2013).
26. Farr, T. G. *et al.* The shuttle radar topography mission. *Rev. Geophys.* **45**, https://doi.org/10.1029/2005RG000183 (2007).
27. Clubb, F. J., Mudd, S. M., Milodowski, D. T., Grieve, S. W. D., & Hurst, M. D. LSDChannelExtraction v 1.0 (Version v1.0). Zenodo, http://doi.org/10.5281/zenodo.824198 (2017).
28. Peel, M. C., Finlayson, B. L. & McMahon, T. A. Updated world map of the Köppen-Geiger climate classification. *Hydrol. Earth Syst. Science. Discuss.* **4**, 439-473 (2007).
29. Trabucco, A. & Zomer, R. J. Global aridity index (global-aridity) and global potential evapo-transpiration (global-PET) geospatial database. CGIAR Consortium for Spatial Information http://www.cgiar-csi.org/data/global-aridity-and-pet-database (2009).
30. Slingerland, R., Harbaugh, J. W. & Furlong, K. *Simulation Clastic Sedimentary Basins: Physical Fundamentals and Computer Programs for Creating Dynamic Systems* (Prentice Hall, Englewood Cliffs, 1994).
31. Seybold, H., Rothman, D. H. & Kirchner, J. W. Climate's watermark in the geometry of stream networks. *Geophys. Res. Lett.* **44**, 2272-2280 (2017).
32. Bonnet, S. Shrinking and splitting of drainage basins in orogenic landscapes from the migration of the main drainage divide. *Nature Geosci.* **2**, 766 (2009).
33. Molnar, P., Anderson, R. S., Kier, G. & Rose, J. Relationships among probability distributions of stream discharges in floods, climate, bed load transport, and river incision. *J. Geophy. Res. Earth Surf.* **111**, https://doi.org/10.1029/2005JF000310 (2006).

Acknowledgements Funding: The time of M.B.S. was partially supported by NSF (BCS-1660490 and EAR-1700555). The authors acknowledge the use of the UCL Legion High Performance Computing Facility (Legion@UCL), and associated support services, in the completion of this work. We thank Rudy Slingerland for sharing the code and providing advice on the LONGPRO model. We thank Jane Willenbring for comments on an early version of the manuscript, as well as three anonymous reviewers for detailed comments that improved the paper.

Author Contributions K.M and M.B.S conceived of the research and designed the study. S.W.D.G. extracted the river long profiles. S-A.C. carried out the data analysis and model simulations. S-A.C., K.M. and M.B.S wrote the manuscript with contributions from S.W.D.G.

Author Information The datasets generated and analyzed during the current study are available here. Any Methods, including any additional references and Extended data, are available in the online version of the paper. The authors declare no competing financial interests: details are available in the online version of the paper. Readers are welcome to comment on the online version of the paper. Correspondence and requests for materials should be addressed to K.M. (katerina.michaelides@bristol.ac.uk).

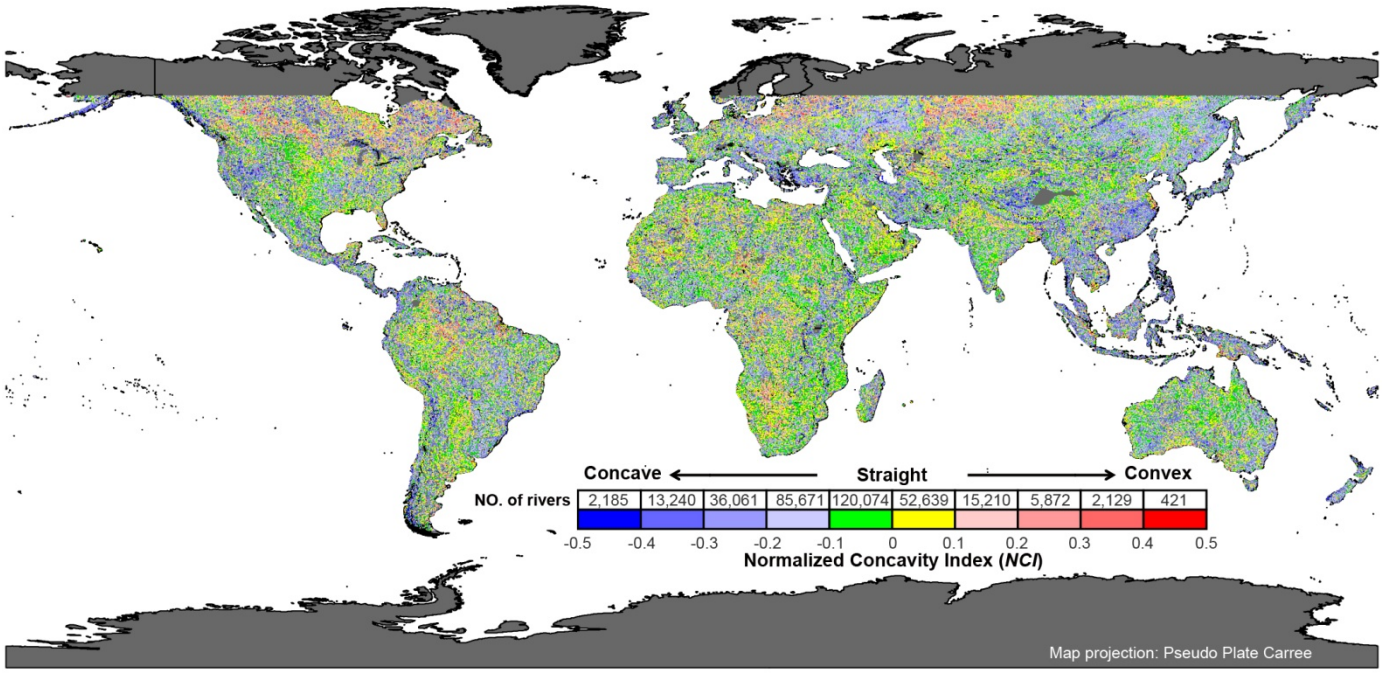

Figure 1 | Global map of extracted river long profiles classified by Normalized Concavity Index (*NCI*) values. Each dot identifies the most downstream point of each extracted river profile, color-coded by *NCI* value. River long profiles were extracted from the 30-m SRTM-DEM, which covers land area between 60° N and 56° S. Inset table shows the number of extracted rivers in each *NCI* bin. (Source of background map: Natural Earth, https://www.naturalearthdata.com/)

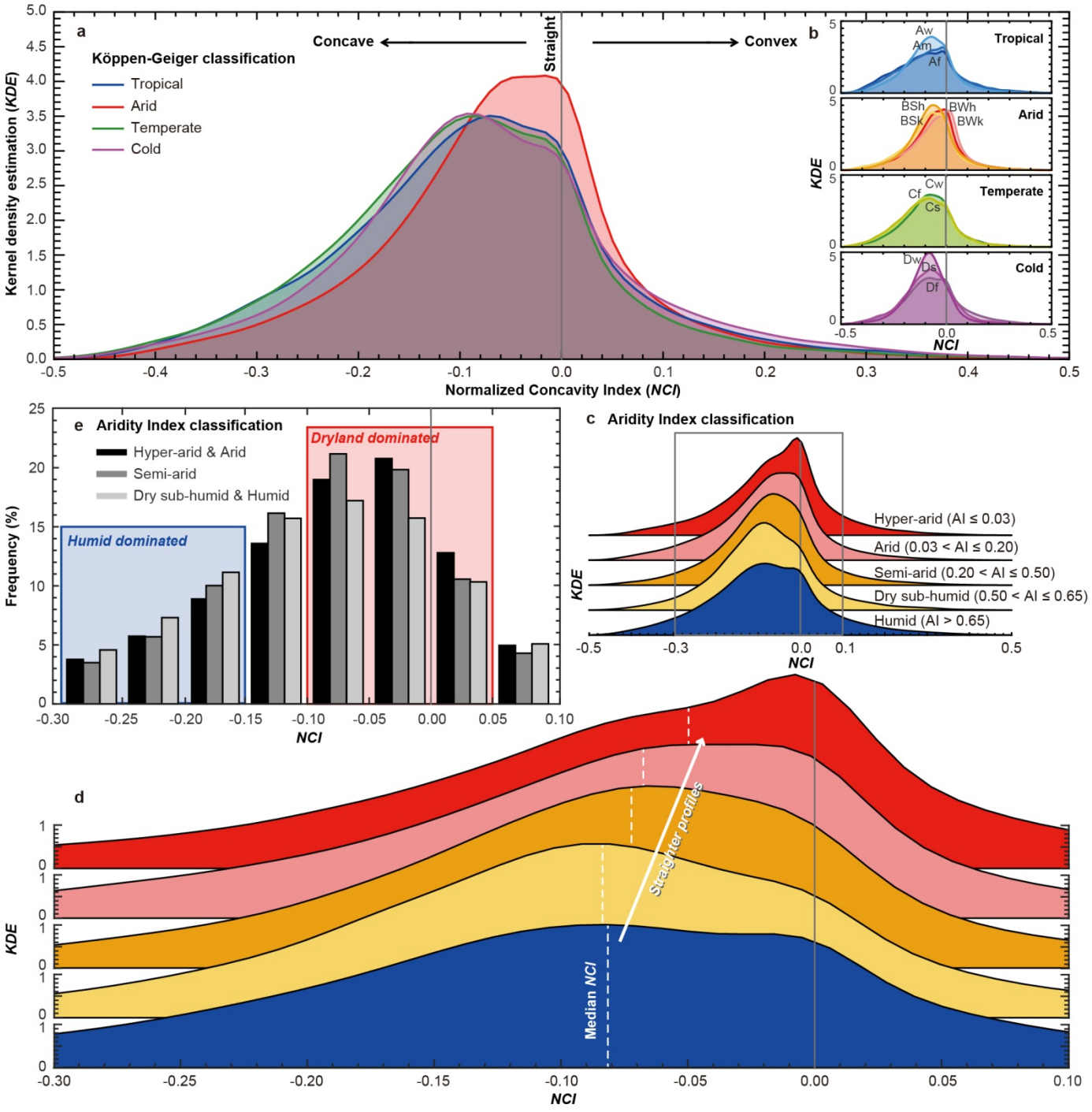

Figure 2 | Effect of climate on *NCI*. Kernel density estimation (*KDE*) is a nonparametric representation of the probability density function. Comparisons of *NCIs* for: **a,** Four main Köppen-Geiger (K-G) climate zones highlighting the distinctiveness of Arid zone concavities; **b,** Sub-zones of K-G classification. **c,** The *KDE* comparison of *NCIs* between climate categories of the Aridity Index (AI). **d,** Enlarged part of the grey frame in panel **c** showing variations in *NCI* distributions based on AI. **e,** Frequencies of combined AI categories between *NCI* distributions highlighting dryland dominated and humid dominated bins of *NCIs*.

271 ‘Dryland’ includes Hyper-arid, Arid, and Semi-arid categories; ‘Humid’ includes Dry sub-humid and

272 Humid.

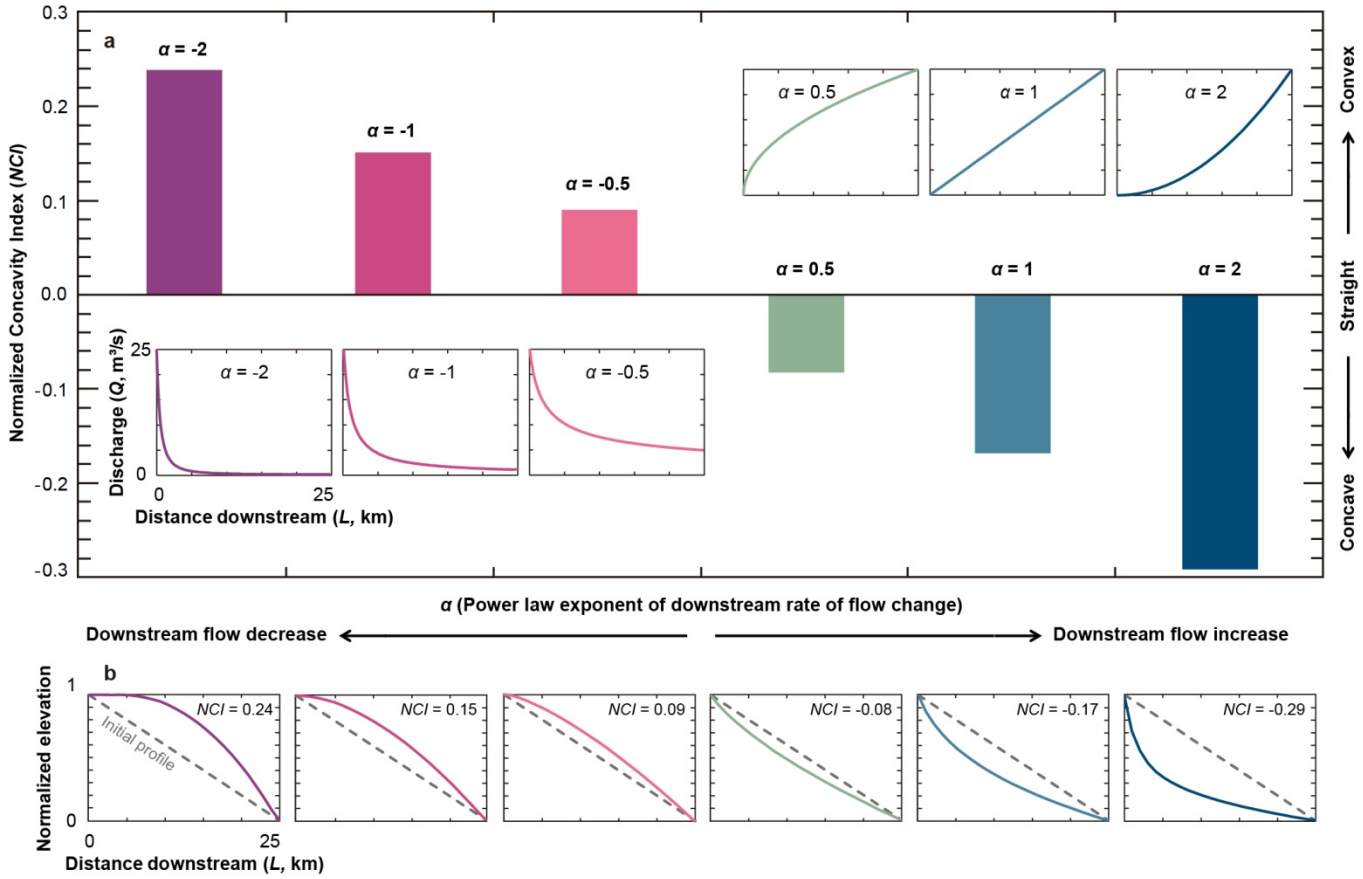

Figure 3 | Modeling river long profiles with various downstream rates of flow change. a, *NCI* values for long profiles simulated with LONGPRO with a range of downstream rates of flow change (α). Inset figures are the corresponding downstream distributions of discharge for various α values used in the LONGPRO modeling. **b,** Simulated river long profiles for the corresponding various α, normalized by total river relief.

METHODS

Köppen-Geiger and Aridity Index Classifications. Our four main Köppen-Geiger (K-G) climate zones[28] were compiled by aggregating the Af, Am, and Aw sub-zones into the Tropical zone; BWh, BWk, BSh, and BSk sub-zones into the Arid zone; Cs, Cw, and Cf sub-zones into the Temperate zone; and Ds, Dw, and Df sub-zones into the Cold zone. We excluded Polar zones from the K-G dataset because of their tendency to be covered by permafrost or glaciers, making them subject to predominantly glacial processes rather than fluvial ones, and due to the latitude constraints of the Shuttle Radar Topography Mission Digital Elevation Model (SRTM-DEM) dataset[26]. We acquired the spatial distribution of Aridity Index (AI) along each river profile from the Global Aridity and PET Database[29], then calculated the median AI value for each river.

One may wonder whether the prevailing climate in any basin may have shifted during or since profile development and how that might affect our results. In this study, we opted to use climate metrics that can currently be measured on a global basis, since they represent the best available information for analysis of a global river profile dataset. Having confirmation from two climatic indices (K-G and AI), which are computed in distinct ways (e.g., AI represents the balance between PET and P), gives us confidence that we have captured real climate influences on long profile development. There will undoubtedly be examples where marked biome/climate shifts occurred during or since profile development within a region. However, since we observed clear relationships between current climate classifications and *NCI*, we believe this makes a strong case for contemporary climatic control on the profile. We suspect that any major climatic changes over or since the period of profile development would merely be captured in the noise of the GLoPro dataset.

River long profile extraction. Using the K-G climate zones[28], the global SRTM-DEM[26] was broken into contiguous climate zone tiles, prior to performing any topographic processing. This ensured that only rivers which were contained within a given climate zone would be extracted, and that any climatic signal contained within river long profile geometry would not be distorted by a river crossing climate zones. This

means that the GLoPro dataset is limited to river basins that are typically <2,500 km^2 in area and <400 km in length (Extended Data Fig.4). In some cases, the contiguous climate zone tiles were still too large to be efficiently processed, and so these tiles were subdivided into smaller tiles using a quadtree algorithm. This processing resulted in 1,366 individual DEM tiles, each with an approximate spatial resolution of 30 meters, which could be processed in parallel. To ensure the validity of measurements of river long profile geometry, and the ability to accurately compare measurements at a global scale, each DEM tile was projected into the appropriate UTM coordinate system. Our method applied to the entire SRTM dataset optimizes the quality and internal consistency of the topographic information extracted into GLoPro, but it comes at the expense of precise geographical information due to spatial variability in projection of the dataset. This means that it may be challenging to match up GLoPro stream locations accurately to GIS stream layers from other databases.

The topographic analysis of each of these tiles was performed using LSDTopoTools[27], an open source topographic analysis package designed to facilitate robust, reproducible analysis of DEM data. The first processing step was to hydrologically correct each DEM tile, to ensure that no artificial sinks were present. This was performed using an algorithm[34] which minimizes the topographic change required to ensure all DEM cells flow to the DEM base level. Following this, each cell in the DEM which exceeded a threshold drainage area, and which had no upslope cells also exceeding the threshold were identified as channel initiation points. The FastScape algorithm[35] was then applied to these initiation points to efficiently route flow downslope in the direction of steepest descent to generate a channel network for each tile. This steepest descent method partitions flow from the DEM cell of interest to one of its 8 neighbouring cells. From this generated network, the highest order river (the longest channel) in each drainage basin or sub-basin, that did not cross K-G sub-zone boundaries (Extended Data Fig.1a), was extracted and incorporated into GLoPro.

Although more elaborate methods for channel extraction exist, it has been shown that these methods perform poorly on 30-m resolution data[36], particularly in the upper reaches of catchments, where channel

329 initiation points are known to be fine scale, transient features[37]. The selection of a threshold drainage area is
330 challenging in any study, with considerable effort being expended on identifying techniques to constrain
331 it[38]. These challenges are also magnified by the scale of this study, where the ideal threshold for a given
332 area may be unsuitable for another. To resolve this issue, a deliberately conservative drainage area
333 threshold of 25,000 pixels, equivalent to an area of 22.5 km^2 at the equator, was applied. This value
334 balances the need for computational efficiency with the requirement to extract the properties of large
335 mainstem rivers in which we can have confidence[36].
336 We were concerned that our extraction method might yield false positives in areas where one would
337 expect few channels (e.g., dune fields such as the Sahara Desert). To check for this, we analyzed the
338 extracted channels from LSDTopoTools for part of The Grand Erg Oriental, Western Sahara. We found
339 that the flow accumulation algorithm results from LSDTopoTools showed flow between dunes along local
340 topographic gradients and a coalescence of flow into a dominant channel that follows the regional
341 topographic gradient (Extended Data Fig.2). This is the channel that was extracted in our analysis for this
342 area and which is included in GLoPro. It is plausible that under heavy rainfall, overland flow runoff would
343 accumulate in this manner and it would coalesce into a dominant channel that reworks dune sediment and
344 leaves behind a topographic signature that is preserved. From arid lands literature on fluvial-aeolian feature
345 interactions, we confirmed that it is common that interdune flow and coalescing flows ("through-going"
346 fluvial channel networks) cross entire aeolian dune fields and leave behind topographic signatures[39].Even
347 after removing all major global dune fields from GLoPro, we determined that our *NCI* results showing
348 systematically straighter long profiles with increasing aridity, are unaffected. It is worth mentioning that the
349 fluvial channels included in GLoPro are based on a topographic definition – they represent a set of
350 contiguous topographic positions in the landscape that would accumulate flow from upstream (should water
351 be present in the landscape) above a conservative threshold drainage area. A single point or a discontinuous
352 series of points defined as a channel trace would not be extracted for inclusion in GLoPro. Instead, the
353 extraction algorithm required a consistent decline in elevation along the flow trace and an accumulation of

upstream drainage area to define a channel. Accordingly, only longer channels in a basin or sub-basin would be included in our database. We view this definition as a conservative one, that would tend to rule out the inclusion of non-channel features (false positives) in our database.

For each DEM cell identified as a channel, topographic information was sampled to facilitate the creation of river long profiles, along with other relevant information about the river channel. This resulted in an average sampling frequency of 36 meters along the length of each river, recording the elevation, flow length, drainage area, latitude and longitude of each cell. In addition to these topographic data, AI values were sampled at the centroid of every cell along the length of each river and the median AI value was calculated for the whole river. There are a small number of cases (40 rivers, or 0.01% of the dataset) where very few AI measurements (<10) were made along a river, caused by the discrepancy between the spatial resolution of the AI data (~900 meters) and the SRTM dataset the rivers are extracted from (~30 meters).

Given their source in SRTM data, the extracted profiles represent the water surface profile for perennial rivers and the bed topography profile for ephemeral rivers. The two profile types are comparable over the entire profile, as the water surface responds to the bed topography. Furthermore, *NCI* robustly captures the overall shape of the longitudinal profile, irrespective of high frequency variations associated with either bed or water surface profiles.

Normalized Concavity Index (*NCI*). We define the endpoints of the longitudinal profile (L_0, E_0) and (L_n, E_n) where L is distance downstream, E is elevation, and where the subscripts 0 and n indicate the most upstream and downstream points, respectively. To calculate *NCI*, a straight line is fitted through the endpoints of the longitudinal profile descibed by the equation $Y_L = E_0 - \theta L$, where Y_L is the elevation on the line at each distance L, θ is the gradient of the line, and E_0 is the y-intercept. Then, at each measured point along the profile, the vertical offset between the river profile and the fitted straight line is calculated as $E_L - Y_L$. We then calculate the median value of all offsets, normalized by the total topographic relief along the profile ($E_0 - E_n$) to enable comparison across scales (Extended Data Fig.1b). Therefore, *NCI* is defined as:

$$NCI = median[(E_L - Y_L)/(E_0 - E_n)] \quad (1)$$

There have been previous concavity indices developed in the literature, such as Stream Concavity Index (*SCI*)[7], Concavity Index (θ)[40], and Chi (χ) transformation[41]. *SCI*, for example, calculates the area between channel elevation and the straight line connecting the endpoints of channel, similar to *NCI*. However, *SCI* is sensitive to local variations along the profile (e.g., knickpoints) and requires smoothing. On the other hand, θ and χ are computed based on local channel gradient and upstream contributing drainage area and they are typically applied to multiple segments along the same river trace, rather than to summarize the concavity of an entire profile. Since our goal was to explore conditions where the relationship between area and channel discharge are weak for complete river profiles, we opted for a different metric. Advantages of *NCI* are that: 1) it calculates all offsets of measured points at the native resolution of the measurements (DEM, field survey, model output); 2) it does not require any smoothing along the profile; 3) it does not require any assumptions about the relationship between slope and area or between area and river discharge; and 4) it can be used to quantify concavity of a simulated profile (devoid of basin area). The calculation of all vertical offsets along the profile enables the representation of local variations along the profile (e.g., knickpoints), but the calculation of *NCI* is not sensitive to them (Extended Data Fig.3 as an example).

The river extraction methods and concavity calculation result in an internally consistent *NCI* dataset. The impact of channel head location on *NCI* is minimal because only the longest river of each basin or sub-basin was analyzed (not smaller tributaries). We confirmed that *NCI* for extracted rivers in GLoPro are not correlated with key river metrics, such as river length, gradient, relief, or basin area (Extended Data Fig.4). Therefore, we were confident in using it to compare rivers of different sizes and across climate zones.

Global Longitudinal Profile (GLoPro) database.

Database Structure

GLoPro is an SQLite database comprising two tables: **rivers**, which has the following columns:

1. uid: A unique ID assigned by the database for each record.
2. riverid: The unique name given to each river record in GLoPro. Comprises the K-G climate zone that the river is within and a unique alphanumeric string. Used to identify a given profile in the profile table.
3. *NCI*: The Normalized Concavity Index.
4. koppen: The K-G climate zone.
5. geom: A GeoJSON string containing the river geometry. Can be imported directly into any modern GIS package (e.g., QGIS). For more information on the GeoJSON format see http://geojson.org.

and **profiles**, which contains:

1. uid: A unique ID assigned by the database for each record.
2. riverid: The unique name given to each river record in GLoPro. Comprises the K-G climate zone that the river is within and a unique alphanumeric string. Used to identify the associated data for the river recorded in rivers.
3. lat (decimal degrees): The latitude of the sampled point. Spatial coordinates correspond to EPSG code 4326.
4. long (decimal degrees): The longitude of the sampled point. Spatial coordinates correspond to EPSG code 4326.
5. length (meters): The cumulative flow length from the outlet of the river.
6. area (square meter): The drainage area at a given point along a river.
7. AI: The AI value for a given point along the river. AI data is from http://www.cgiar-csi.org/data/global-aridity-and-pet-database.

Example Queries

To select all of the data from the rivers table:

*SELECT * FROM rivers;*

To select all of the data from a given climate zone:

*SELECT * FROM rivers WHERE koppen like 'Af';*

To select rivers which have an NCI below a value:

SELECT riverid FROM rivers where NCI < -0.1;

To select the elevation and flow length of a given river, which can be used to plot a long profile:

SELECT elevation, length FROM profiles WHERE riverid like 'Aw_75_river_72';

Note that due to the size of the **profiles** table, queries can take a few minutes to complete. To learn more about using SQL databases in a research context, the authors recommend the training materials provided by Software Carpentry: http://swcarpentry.github.io/sql-novice-survey.

Kernel density estimation (*KDE*). In several figures in the paper, we present plots generated based on kernel density estimation (*KDE*). *KDE* is a nonparametric representation of the probability density function for the sample data. To show the distribution of *NCI* values of each climate zone, we used the built-in function, ksdensity, in MATLAB. Since the bandwidth of the kernel smoothing window affects the distribution shape, which leads to a smoother shape at higher bandwidth, we kept bandwidth constant at an appropriately smoothed value of 0.02 for all climate zones (Fig.2). However, we also tested the estimations with various bandwidths for K-G classification, from 0.005 to 0.04. All results show that *NCI* distributions of the Arid zone skewed toward zero compared to three main humid zones, irrespectitve of the choice of bandwidth.

Two-sample Kolmogorov-Smirnov test. Statistical differences of the *NCI* distributions were analyzed using the Kolmogorov-Smirnov test (K-S test) between distribution pairs across climate zones. K-S test is a

nonparametric test for checking whether two continuous, one-dimensional data samples, X_1 and X_2, come from the same distribution. We used the built-in function, kstest2, in MATLAB to calculate the statistic and corresponding p-values between K-G and AI categories (Extended Data Fig.5). Since the number of sampled rivers is very large, p-values of all comparisons are lower than 2.1×10^{-20}. However, in K-G climate zones, comparisons between humid zones and the Arid zone yield p-values lower than 4.27×10^{-190} (Extended Data Fig.5a). Within the AI classes, smaller p-values result when comparing categories that are further apart in terms of aridity (e.g., Hyper-arid zone v. Humid zone) (Extended Data Fig.5b). These results support the conclusion that long profile shapes are very significantly different between arid and humid regions.

LONGPRO modeling. LONGPRO is a one-dimensional numerical model for simulating the dynamic evolution of the river long profile, and can be used to explore responses to varying water discharge, sediment supply, bed grain size, tectonic uplift, and base level[30]. LONGPRO includes: 1) gradually varied flow; 2) sediment transport by Yang's unit stream power equation[42]; and 3) conservation of mass. We used LONGPRO to explore the relative controls on longitudinal profile development. Our goal was not to exhaustively explore the parameter space of LONGPRO, but rather to look at first-order effects of downstream discharge variation on the profile development for transport-limited conditions in a manner that is analogous to the supply-limited case generalized by stream power incision theory.

Given the large variance in drainage basin properties across the globe, we fixed several parameters in LONGPRO in order to isolate the effects of the climate expression within streamflow, and the corresponding impact on long profile evolution. We assumed no tectonic uplift and no base level change (but see below for a sensitivity analyses to these and other factors). We set river length to 25 km, a value similar to the median value of all extracted rivers (26.7 km). We set initial profile slope to 0.003, representing an linearly decline from 75 m elevation at the upstream profile point (i.e., E_0) to 0 m at the downstream point (E_n). Base level (elevation of river water level above the riverbed at the most downstream point) was set at a constant value of 5 m. The maximum water discharge (Q_{max}) was set as

25 m^3/s. Sediment-related parameters in LONGPRO include sediment supply at the upstream boundary (*MFEED*), sediment concentration of lateral inflow to the mainstem (*SEDCON*), the median grain size of bed material (*DIMID*), and Manning's roughness coefficient (*n*). For these parameters, we set the following values as constants: *MFEED* to 10 kg/s, *DIMID* to 1 mm (uniform grain size along the profile), and *n* to 0.04. *SEDCON* was set to 0.00005 (proportion of sediment concentration delivered by lateral tributary inputs), which follows the formula:

$$q_{s,L} = SEDCON(Q_L - Q_{L-1})(\Delta t) \quad (2)$$

where $q_{s,L}$ is the mass of lateral sediment supply at the distance downstream, L, which enters over timestep, Δt. Note: for downstream-decreasing discharge, we exchanged the positions between Q_L and Q_{L-1} in formula (2), in order not to get a negative q_s. The distance between calculated nodes was set as 1 km, and the timestep, Δt, was set to 24 hours. The models were run for 500 years of effective discharge, by which time the rate of change to the profile became relatively small. In fact, the model tended to adjust to near steady-state conditions very rapidly, rendering the model results insensitive to the initial profile, as per the model's design[30]. Since effective discharge tends to be expressed for much briefer periods (e.g., bankfull discharge often is assume to have a return period of ~1.5 years), the model simulation time actually represents a much longer period of topographic adjustment.

We varied downstream rate-of-change in streamflow, α, to explore the effects of climatically driven streamflow on long profile evolution in LONGPRO. In order to do this, we modified the LONGPRO code to enable the power law exponent, α, to vary from positive to negative values:

$$Q_L = Q_n(L/L_n)^{\alpha} \quad (3)$$

where Q_L is the discharge at the distance downstream, L, Q_n is the discharge of the most downstream point, and L_n is the river length. For downstream increasing discharge, Q_n equals Q_{max} (25 m^3/s). However, for downstream decreasing discharge, Q_{max} occurs at the most upstream point (Q_0) and Q_n is calculated from equation (3) for the given α value. In this manner, we simulated variations in downstream discharge and their impact on long profile evolution. For each simulation, we generated a longitudinal profile for which

504 we calculated the *NCI*. A range of simulated profiles from LONGPRO and associated *NCI* values for
505 varying values of α are shown in Fig.3.

506 Since other model parameters can also affect long profile concavities, we conducted sensitivity analyses
507 to discharge (Q_{max}), median grain size (*DIMID*), tectonic uplift, and base level change. To model tectonic
508 uplift in LONGPRO, we applied the maximum uplift rate at the most upstream point (0.1 mm/y and 1
509 mm/y), and the rate decreased linearly downstream to zero at the most downstream point. To model base
510 level change, LONGPRO uses a simple sine function to represent base level variation. We set the amplitude
511 and period of the sine curve to represent continuous base level decline (10 mm/y and 50 mm/y). The results
512 of these various sensitivity analyses show that α is the dominant control of long profile concavity
513 overprinting other factors (Extended Data Fig.6). Moreover, the other exogenous factors that are often
514 assumed to control long profile evolution have a lesser effect than the expression of downstream hydrology.
515 **Calculation of α values from real rivers.** To develop a real-world understanding of α and its variation in
516 different climate zones, we downloaded multidecadal mean daily streamflow data for rivers from the US
517 Geological Survey's National Water Information System (https://waterdata.usgs.gov/nwis). For each main
518 K-G climate zone, we selected 5 rivers, spanning a range of river lengths, with at least three gauging
519 stations along the same river (a total of 20 rivers), ensuring via Google Earth satellite imagery that there are
520 no obvious anthropogenic factors that could influence the downstream variation in discharge. The K-G
521 classification was used as a mask for river selection by climate zones within the USA. The selected rivers
522 needed to fulfill the following criteria: 1) at least three gauging stations for calculating α values; 2) no
523 apparent influence of urban areas affected by irrigation or dams; and 3) no crossing between main K-G
524 climate zones. Of these 20 rivers, three rivers are within the US Department of Agriculture-Agricultural
525 Research Service's experimental watershed network (https://www.fs.usda.gov/treesearch/pubs/50873)[43].
526 We selected rivers distributed over different states with various lengths.

527 The median AI of each river was calculated to compare to K-G climate zones (Extended Data Table 2).
528 We calculated the median discharge for each gauge over the record, and then estimated a best-fit power law

529 trendline to these discharges versus distance downstream for each river (Extended Data Fig.7). Then we
530 extracted α for each power law fit from equation (3) (Extended Data Table 2).

531 The results show that rivers in Tropical, Temperate and Cold zones exhibit median α values between
532 1.24 and 1.75 (downstream increasing discharge), while the Arid zone displays α values that span negative
533 (downstream decreasing discharge) and positive (downstream increasing discharge) with a median close to
534 zero ($\alpha = 0.14$) (Extended Data Fig.8a).

535 We also used these data (82 gauging stations in 20 rivers) to explore the relationship between discharge
536 and basin area. The result clearly shows strong differences between humid zones and arid zones. The
537 former shows a positive relationship between discharge and basin area ($Q = 0.02A^{0.91}$, $R^2 = 0.73$), while the
538 latter shows a very weak dependency on area ($Q = 0.04A^{0.10}$, $R^2 = 0.01$). One recent study[20] extracted flow
539 records from a wide range of US rivers across climate zones and analyzed the exponent of drainage area to
540 discharge. That analysis showed that the exponent on area decreases: 1) with lower mean annual
541 precipitation; and 2) as flood recurrence interval increases, probably due to decreasing probability of storms
542 capable of generating runoff over progressively larger basin areas. The exponent for arid channels is closest
543 to zero for small floods and increases slightly for higher flood recurrence intervals. This is the opposite of
544 the trends in area exponents for humid rivers. This independent analysis result supports our assumption
545 about arid land hydrology, where the relationship between drainage area and discharge is weak. In other
546 words, basin shape is less influential on discharge in arid zones.

547 However, the analysis of α values was not exhaustive. It was based on a small sample of rivers where
548 there was sufficient data to make calculations. In addition, α is based on the full distribution of downstream
549 variations in discharge over decadal timescales. This distribution will not dramatically change α between
550 flood events for perennial rivers in humid climates. In contrast, α in dryland ephemeral channels will
551 fluctuate flood-to-flood between positive and negative values depending on the size, location, and duration
552 of each storm and the runoff it generates. It will also be influenced by the ephemerality (e.g., the length of
553 time between flows) (Extended Data Fig.8b). Nevertheless, these results show the relative differences

554 between α values between groups of rivers in different climate categories, which support our selection of α
555 values used in LONGPRO simulations.
556 **Code availability.** The code for river long profile extraction (LSDTopoTools), including the code for
557 calculating *NCI*, is available on GitHub (https://github.com/sgrieve/concavity). The code for the
558 LONGPRO model is available on Community Surface Dynamics Modeling System (CSDMS,
559 https://csdms.colorado.edu/wiki/Model:LONGPRO). The datasets generated and analyzed during the
560 current study are available here.
561

562 34. Wang, L. & Liu, H. An efficient method for identifying and filling surface depressions in digital
563 elevation models for hydrologic analysis and modelling. *Int. J. Geogr. Inf. Science* **20**, 193-213
564 (2006).
565 35. Braun, J. & Willett, S. D. A very efficient O (n), implicit and parallel method to solve the stream
566 power equation governing fluvial incision and landscape evolution. *Geomorphology* **180**, 170-179
567 (2013).
568 36. Grieve, S. W., Mudd, S. M., Milodowski, D. T., Clubb, F. J. & Furbish, D. J. How does
569 grid-resolution modulate the topographic expression of geomorphic processes? *Earth Surf. Dyn.* **4**, 627
570 (2016).
571 37. Montgomery, D. R. & Dietrich, W. E. Where do channels begin? *Nature* **336**, 232 (1988).
572 38. Tarboton, D. G., Bras, R. L. & Rodriguez-Iturbe, I. On the extraction of channel networks from digital
573 elevation data. *Hydrol. Process.* **5**, 81-100 (1991).
574 39. Al-Masrahy, M. A. & Mountney, N. P. A classification scheme for fluvial–aeolian system interaction
575 in desert-margin settings. *Aeolian Res*. **17**, 67-88 (2015).
576 40. Flint, J. J. Stream gradient as a function of order, magnitude, and discharge. *Water Resour. Res.* **10**,
577 969-973 (1974).
578 41. Royden, L. H., Clark, M. K. & Whipple, K. X. Evolution of river elevation profiles by bedrock
579 incision: Analytical solutions for transient river profiles related to changing uplift and precipitation
580 rates. *Eos Trans. AGU.* **81**, Fall Meet. Suppl., Abstract T62F-09 (2000).
581 42. Yang, C. T. Incipient motion and sediment transport. *J. Hydraul. Div.* **99**, 1679-1704 (1973).
582 43. Goodrich, D. *et al.* The USDA-ARS experimental watershed network-evolution, lessons learned, and
583 moving forward. *Headwaters to Estuaries: Advances in Watershed Science and Management*

584 (Proceedings of the Fifth Interagency Conference on Research in the Watersheds). 54-60 (USDA
585 Forest Service, 2016).

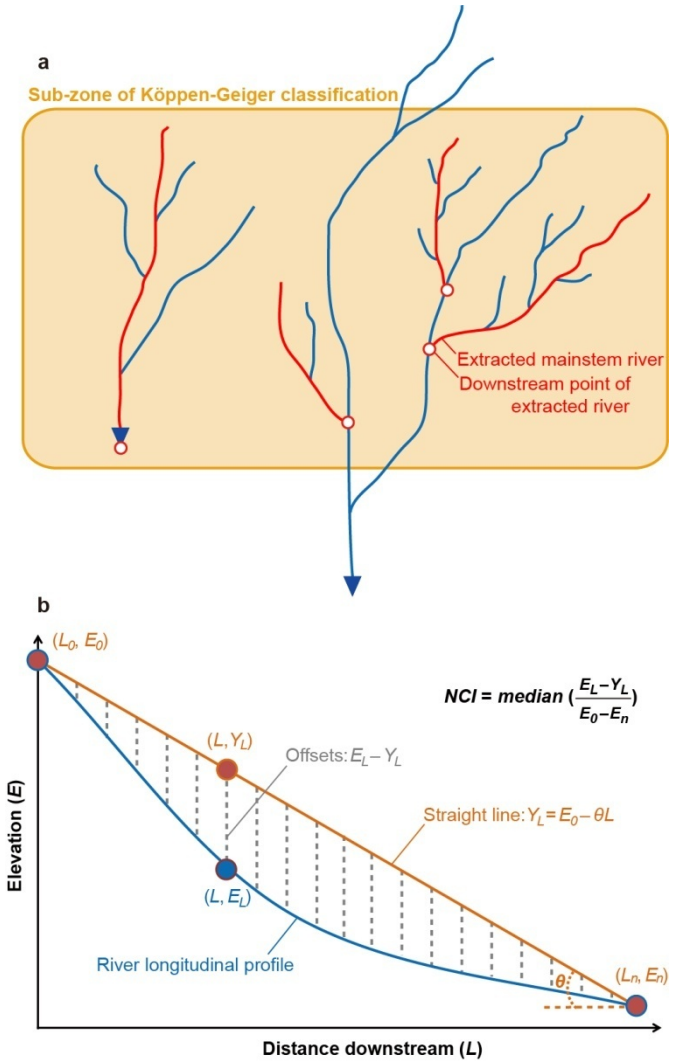

Extended Data Figure 1 | Schematic of GLoPro river selection and *NCI* calculation. a, For each drainage basin, we selected the longest river which does not cross between K-G sub-zones. The schematic drainage system shows the rivers above the threshold drainage area in red (Methods), which were extracted into the GLoPro database. Extracted rivers could include the mainstem river of a whole basin (left) and/or its sub-basins (right). The longest river on the right panel (blue line) was not extracted, since it crosses K-G climate sub-zones. **b,** The blue line is a measured or modeled river long profile, and the orange line is the straight line fitted through the profile endpoints. The offset ($E_L - Y_L$) is the difference of elevations between the river long profile (E_L) and the straight line (Y_L) at each distance L. *NCI* is the median value of all offsets divided by topographic relief ($E_0 - E_n$). *NCI* is negative when the profile is concave, zero when the profile is straight, and positive if the profile is convex.

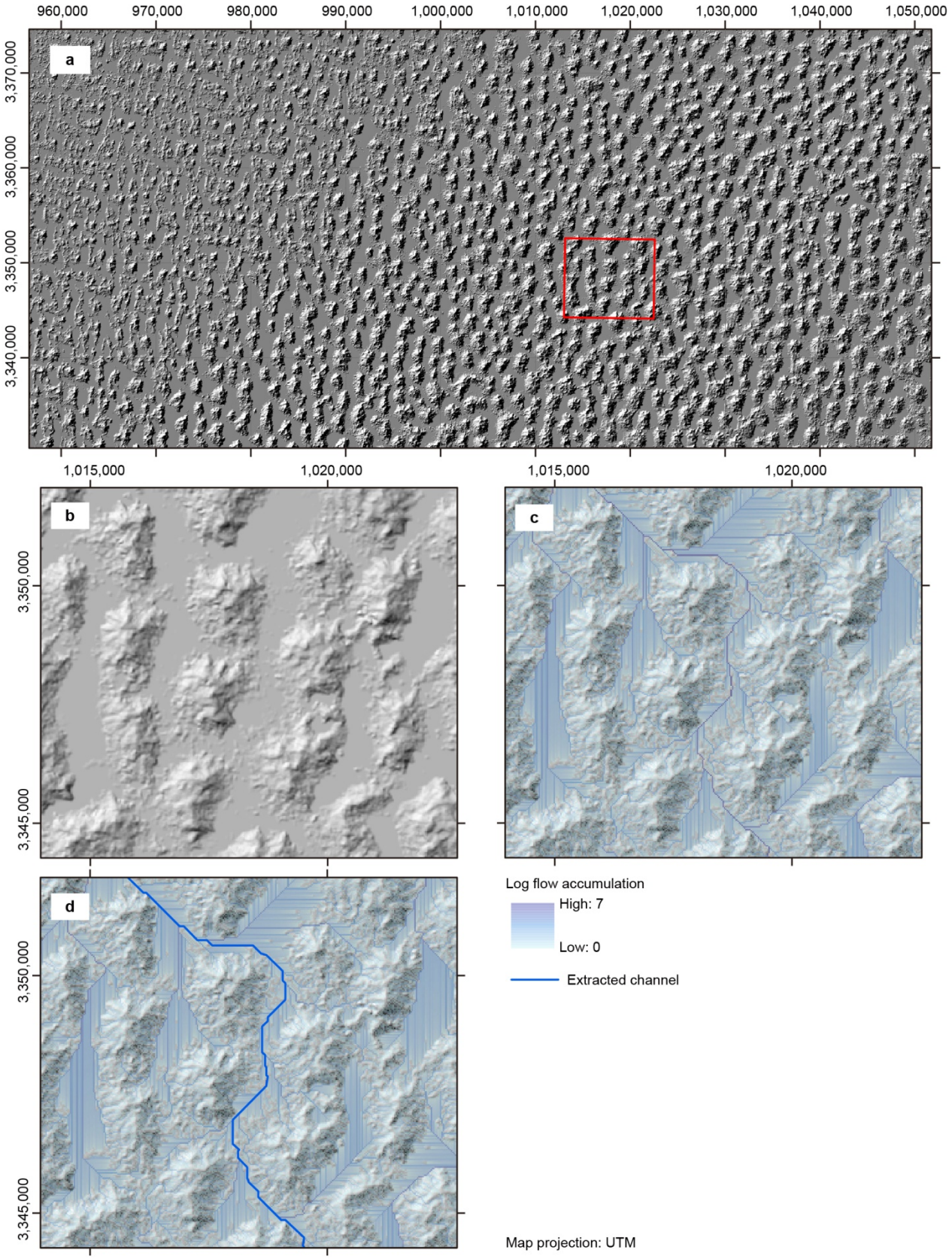

Extended Data Figure 2 | Flow accumulation in The Grand Erg Oriental, Western Sahara. a, The wider context of the area. **b,** The close up of the red frame in panel **a**. **c,** Flow accumulation traces derived

600 from LSDTopoTools. **d,** The extracted mainstem channel in the area representing the coalescence of flow
601 traces into a dominant channel based on topography.

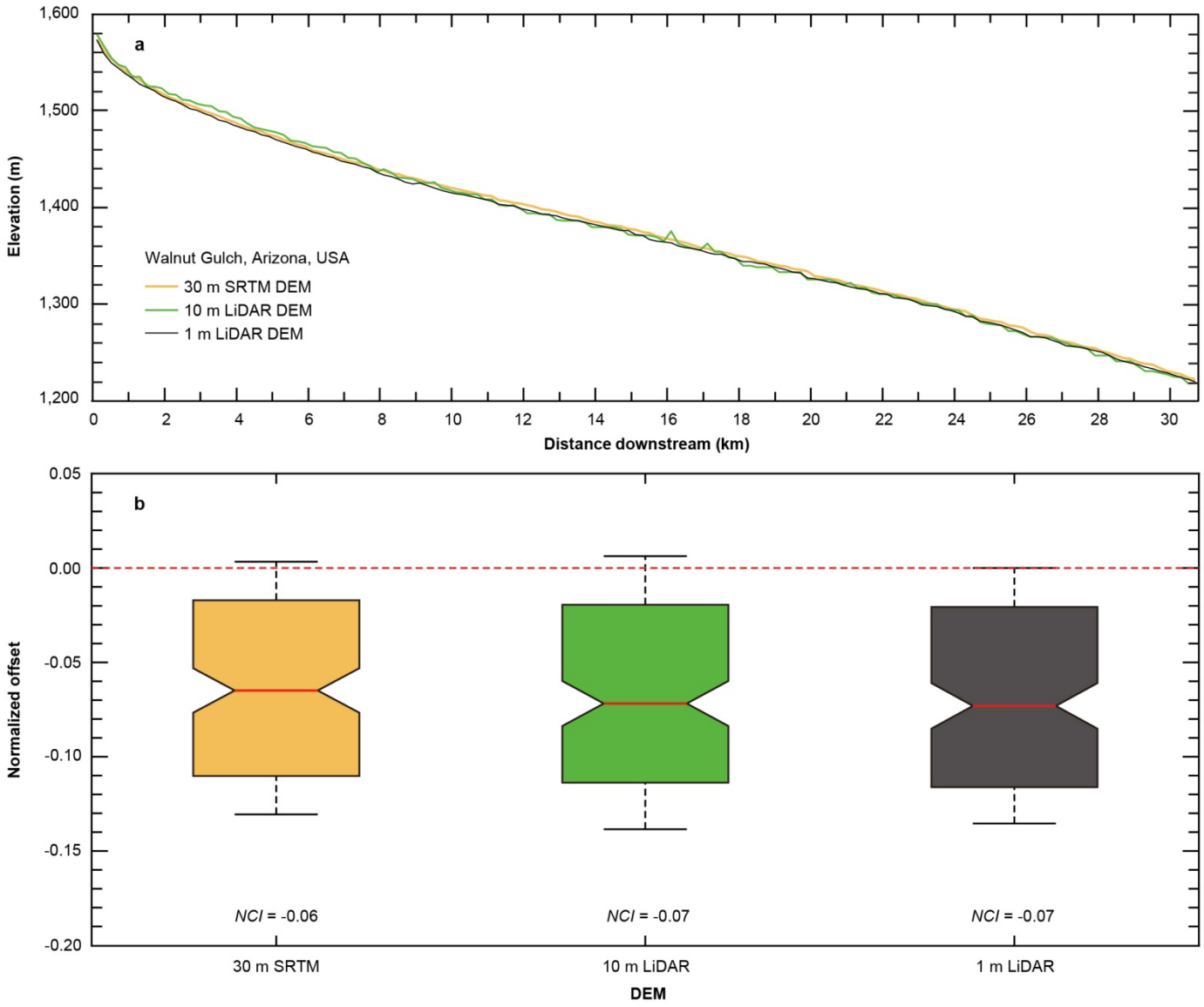

Extended Data Figure 3 | River long profiles and *NCI* values for Walnut Gulch extracted from DEMs of varying resolutions. a, River long profiles extracted from DEMs with different resolutions. **b,** Comparison of normalized offsets between river long profiles and the straight lines fitted profile endpoints. Positive offsets indicate that the elevation of river long profile is higher than the straight line, while negative values mean the elevation of long profile is lower. The red dashed line indicates zero *NCI* (straight profiles). The red solid line in each boxplot represents the median offset value, which we define as the *NCI* value. These profiles show that DEM resolution has a minimal influence on *NCI*.

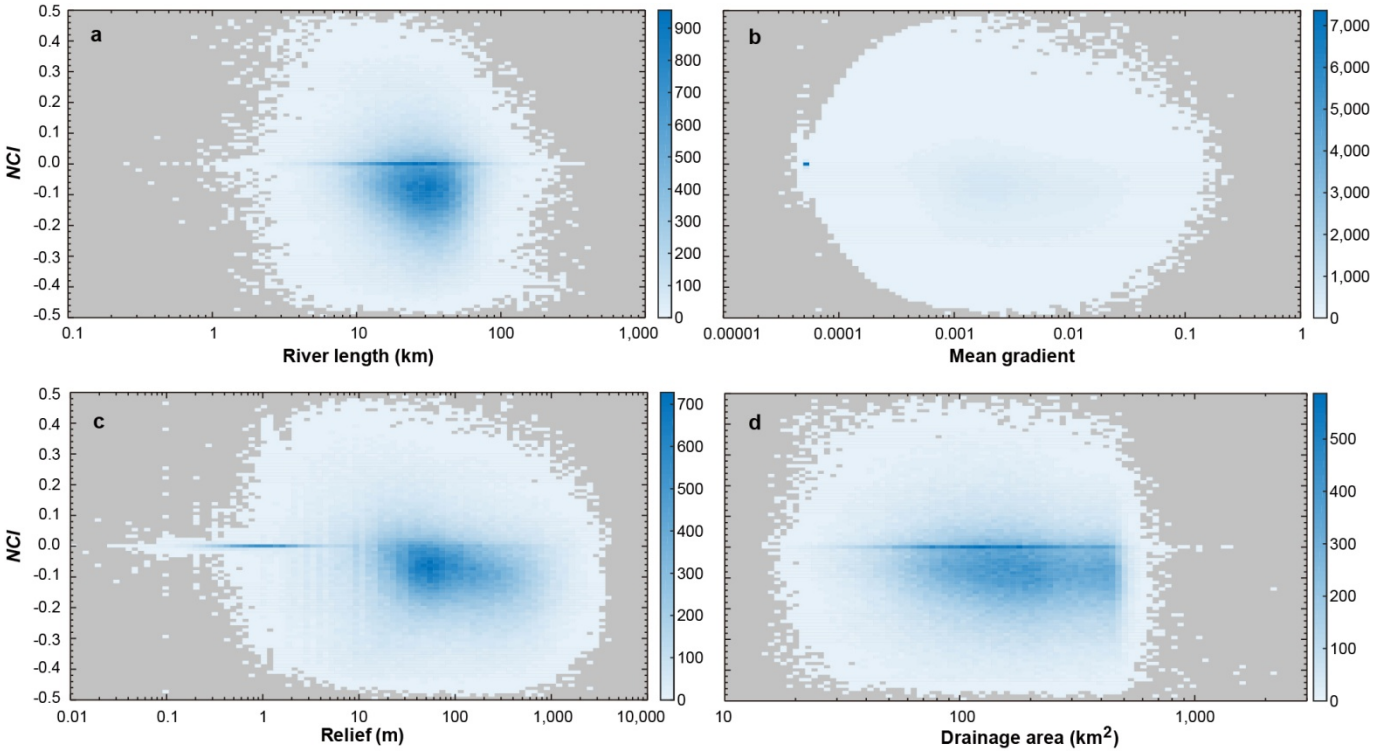

Extended Data Figure 4 | Relationships between *NCI* and topographic metrics. Relationships between *NCI* and: **a,** River length; **b,** River gradient; **c,** River relief; and **d,** Drainage area. Density of points (number of rivers represented by each pixel) in the scatter plot is shown in the scale bars to the right of each panel. The results show no apparent relationship between *NCI* and any of topographic metrics, suggesting *NCI* is unbiased.

Extended Data Table 1 | Summary data on the number of rivers and summary statistics of *NCI* by K-G and AI climate classifications.

K-G climate sub-zone	Af	Am	Aw	BWh	BWk	BSh	BSk	Cs	Cw	Cf	Ds	Dw	Df	All
Number of rivers	13,319	10,020	35,950	50,760	17,697	18,775	26,132	6,983	16,654	25,002	3,476	20,213	88,521	333,502
K-G climate main zone	**Tropical**			**Arid**				**Temperate**			**Cold**			
Number of rivers	59,289			113,364				48,639			112,210			
K-G climate sub-zone	**Af**	**Am**	**Aw**	**BWh**	**BWk**	**BSh**	**BSk**	**Cs**	**Cw**	**Cf**	**Ds**	**Dw**	**Df**	**All**
Median of *NCI*	-0.083	-0.073	-0.081	-0.058	-0.067	-0.063	-0.075	-0.106	-0.080	-0.098	-0.083	-0.105	-0.070	-0.076
K-G climate main zone	**Tropical**			**Arid**				**Temperate**			**Cold**			
Median of *NCI*	-0.080			-0.064				-0.093			-0.080			
K-G climate sub-zone	**Af**	**Am**	**Aw**	**BWh**	**BWk**	**BSh**	**BSk**	**Cs**	**Cw**	**Cf**	**Ds**	**Dw**	**Df**	**All**
IQR of *NCI*	0.188	0.176	0.141	0.130	0.147	0.120	0.141	0.161	0.150	0.157	0.142	0.110	0.158	0.150
K-G climate main zone	**Tropical**			**Arid**				**Temperate**			**Cold**			
IQR of *NCI*	0.159			0.135				0.157			0.154			

AI climate zone	Hyper-arid	Arid	Semi-arid	Dry sub-humid	Humid	All
Number of rivers	21,070	56,571	63,925	33,499	156,759	331,824
Median of *NCI*	-0.050	-0.068	-0.073	-0.084	-0.082	-0.075
IQR of *NCI*	0.131	0.141	0.130	0.138	0.163	0.150

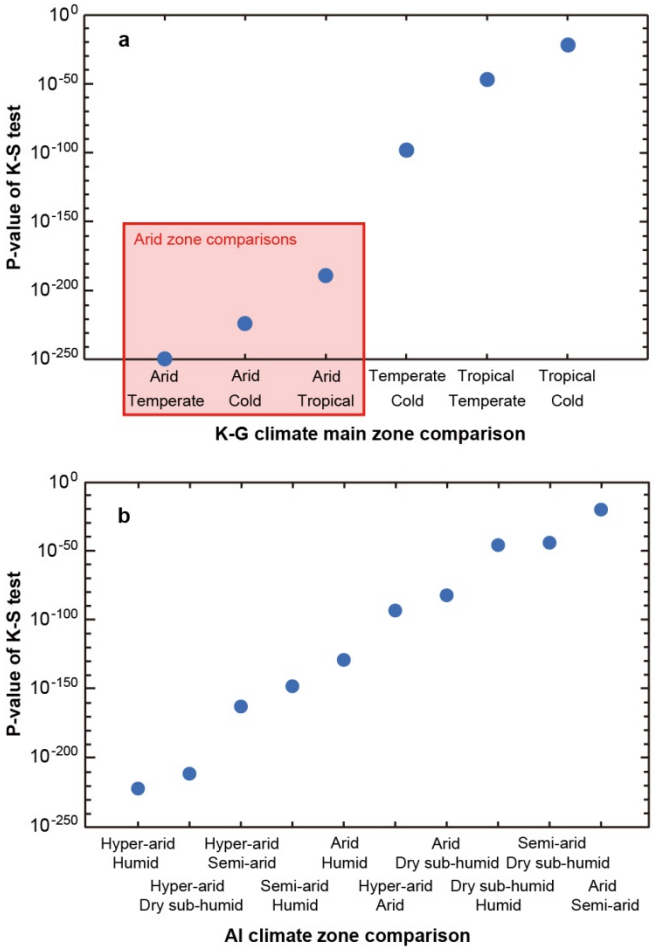

Extended Data Figure 5 | Statistical differences of *NCI* distributions between climate zones. These figures show graphical results of two-sample Kolmogorov-Smirnov tests, which including the p-values of *NCI* comparisons within: **a**, Main K-G climate zones; and **b**, AI climate categories. The red box in panel **a** shows the comparisons involving the Arid zone, which all have smaller p-values compared to other comparisons.

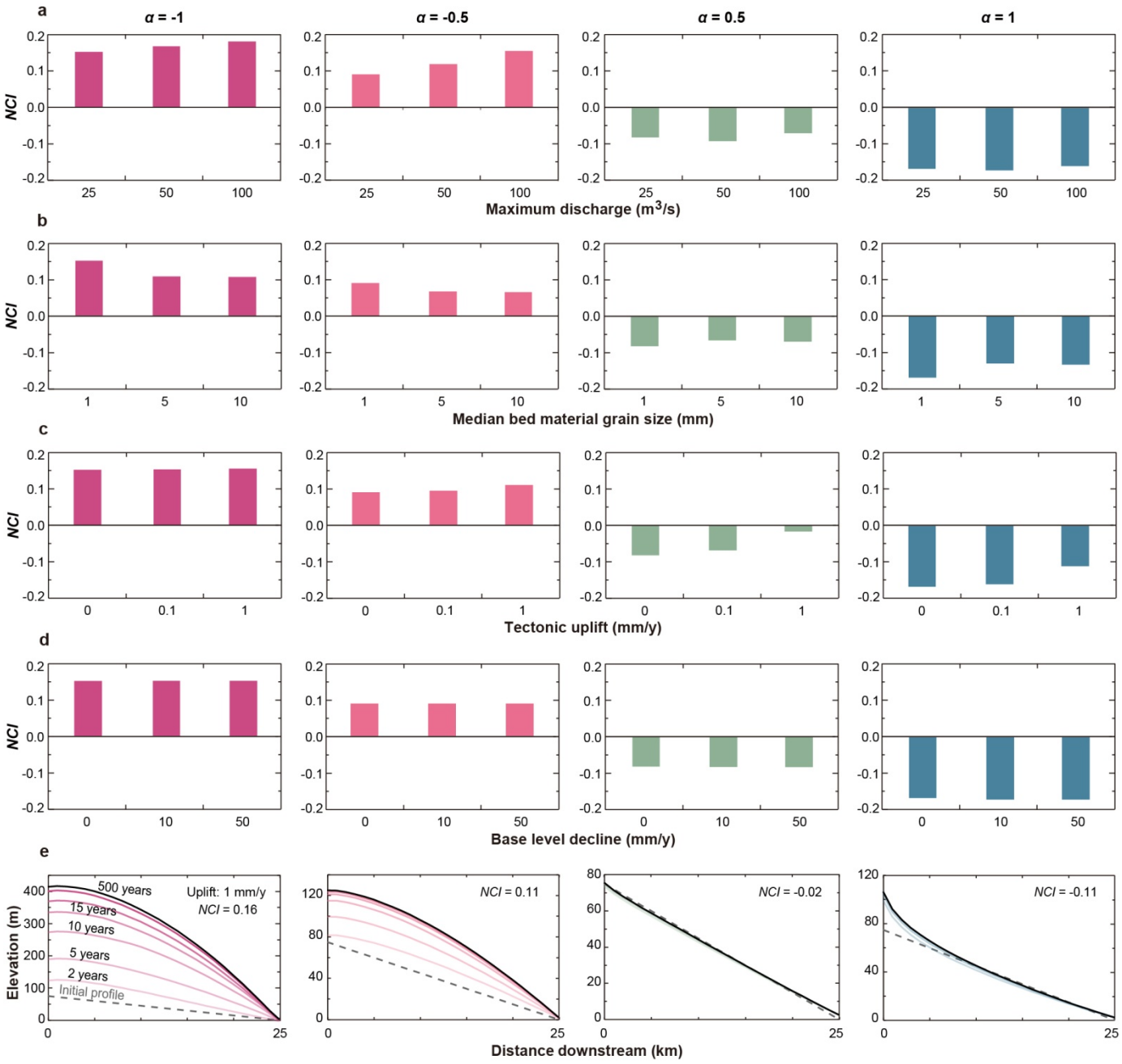

625

626 **Extended Data Figure 6 | Modeled *NCI* values for river long profiles generated with different**

627 **forcings for various *α* values.** *NCI* values for long profiles simulated by LONGPRO with various values

628 of: **a,** Maximum discharge; **b,** Median bed material grain sizes (uniform); **c,** Tectonic uplift rates of the

629 headwater; and **d,** Base level decline rates. All plots highlight the dominant role of *α* on the river concavity.

630 **e,** Long profile evolution with tectonic uplift (1 mm/y), in which the profiles are shown for initial profile

631 (dashed line, the same for all simulations), 2, 5, 10, 15, 20, 30, and 500 years. The final simulated profile

for each is indicated as a dark black line. The *NCI* values of final profiles for each case of α are also shown. Profiles evolve rapidly to near-steady state conditions for all simulations.

Extended Data Table 2 | Data on α and ephemerality (% time with no flow, 'Ephe.') for twenty rivers spanning the four main K-G climate zones within the USA.

K-G zone	AI zone (AI value)	River name	State	Stations	Drainage area (km^2)	River length (km)	Q_n (m^3/s)	Ephe. (%)	α
Af	Humid (1.39)	Rio Tanama	Puerto Rico	50027850 50028000 50028400	57.50	39.93	2.22	0	1.03
Af	Humid (2.45)	Waikamoi Stream	Hawaii	16552800 16554000 16555000 16556000	10.31	11.62	0.29	0-1	3.55
Af	Humid (2.50)	Wailuku River	Hawaii	16701750 16701800 16703000 16704000 16713000	635.79	37.89	4.12	0-4	5.15
Af	Humid (2.49)	Waialae Stream	Hawaii	16019000 16020000 16021000	21.37	18.51	0.44	0-1	0.85
Am	Humid (1.15)	Rio Guayanes	Puerto Rico	50082800 50083500 50085100	68.89	21.17	1.63	0	1.51
BWh	Arid (0.13)	Fortymile Wash	Nevada	10251242 10251250 10251255 10251258	818.44	74.59	0.029	99.6-99.8	-3.18
BSh	Semi-arid (0.33)	Sycamore Creek	Arizona	09510070 09510080 09510150 09510200	424.76	50.12	0.02	4-23	0.85
BSk	Arid (0.18)	Rio Puerco	New Mexico	08333500 08334000 08352500 08353000	16,109.73	369.01	0.21	45-57	0.49
BSk	Semi-arid (0.27)	Limpia Creek	Texas	08431700 08431800 08432000	784.77	66.67	0.013	30-82	-1.23
BSk	Semi-arid (0.22)	Walnut Gulch	Arizona	FL001 FL002 FL006 FL009	149.33	30.80	0.46	96-97	0.14
Cs	Humid (1.69)	South Fork Coquille River	Oregon	14324600 14324700 14324900 14325000	437.71	55.35	7.91	0	1.64
Cs	Humid (1.39)	Redwood Creek	California	11481500 11482000 11482120 11482200 11482500	717.43	95.85	9.16	0	1.24
Cf	Humid (1.11)	Alaqua Creek	Florida	02366996 02367000 02367006	216.78	29.09	4.68	0	1.03
Cf	Dry sub-humid (0.59)	Little Washita River	Oklahoma	07327442 07327447 07327490 07327500 07327550	600.88	56.44	0.62	0-6	1.04
Cf	Humid (0.85)	Little River	Georgia	02317797 02318000 02318380	2,009.83	111.19	4.06	0-19	1.76
Ds	Humid (1.04)	East Fork Pine Creek	Idaho	12413360 12413370 12413445	189.59	13.61	1.52	0	2.02
Df	Humid (1.00)	Susitna River	Alaska	15291000 15291500 15291700 15292000 15292780 15294350	50,142.17	463.34	364.31	0	1.65
Df	Dry sub-humid (0.51)	Middle Loup River	Nebraska	06775000 06775500 06777000 06777500 06778000 06779000 06779500 06780000 06785000	8,106.66	365.24	31.75	0	1.07
Df	Humid (1.17)	White River	Vermont	01142000 01143500 01144000	1,787.09	82.45	18.17	0	1.84
Df	Humid (1.12)	Tionesta Creek	Pennsylvania	03017000 03017500 03018000 03019000	1,214.70	75.17	21.82	0	1.75

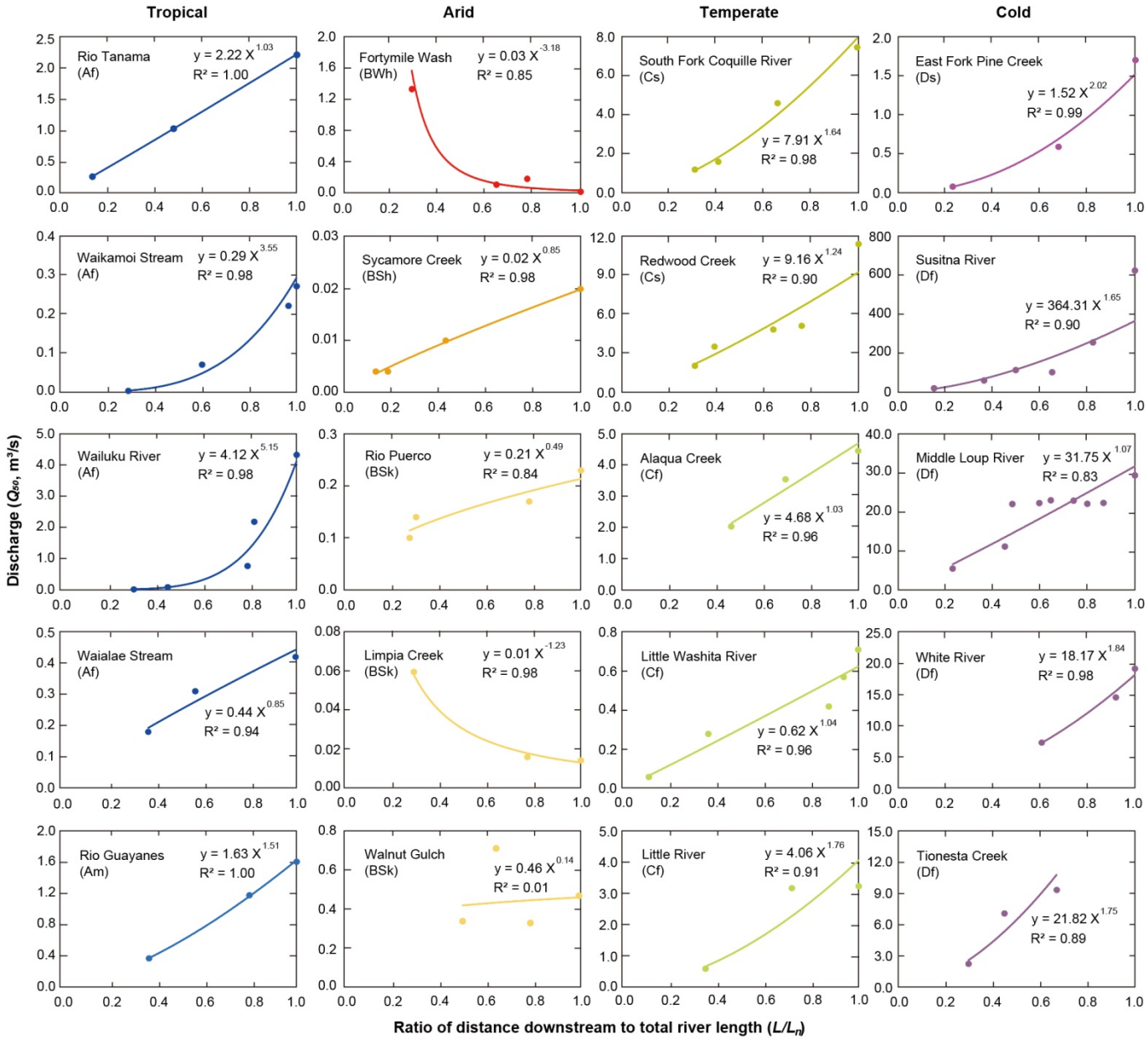

637

638 **Extended Data Figure 7 | Calculation of α values from discharge data.** Power law fits between median

639 daily discharge and L/L_n (equation 3, Methods) for each gauge are shown for the selected rivers within four

640 main K-G climate zones in the USA (Extended Data Table 2). The colors correspond to the K-G climate

641 classification (Fig.2).

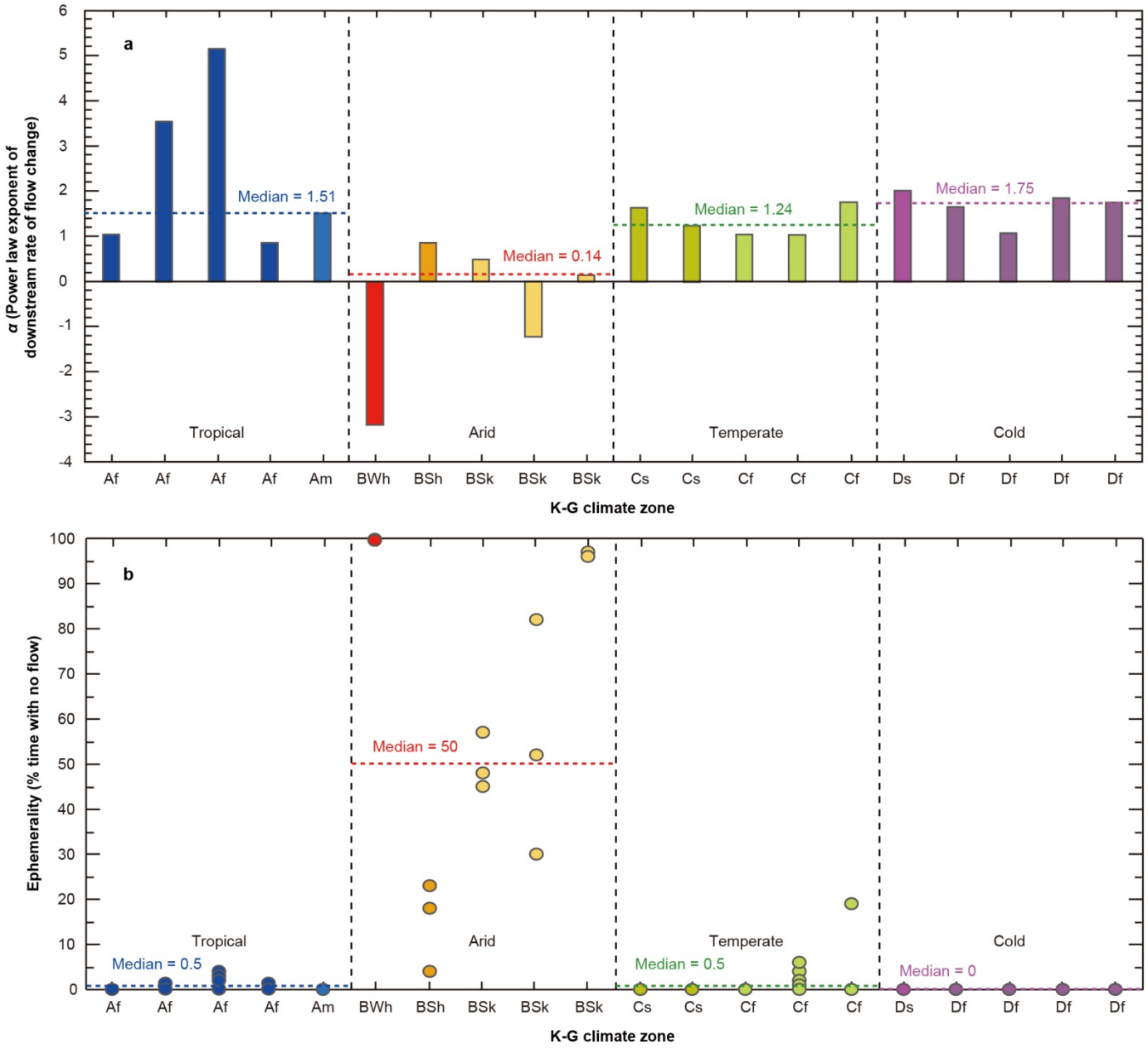

Extended Data Figure 8 | Comparison of α and ephemerality for selected rivers between main K-G climate zones in the USA. a, α values for each selected river; **b,** Corresponding values of ephemerality. The order of rivers is consistent with the data in Extended Data Table 2. The colors correspond to the K-G climate classification (Fig.2). Dotted lines indicate the median value for each main climate zone, showing that Arid zone has lower α and higher ephemerality compared to the others.